Magnetoresistive Conductive Polyaniline–Barium Titanate Nanocomposites with Negative Permittivity

ARTICLE *in* THE JOURNAL OF PHYSICAL CHEMISTRY C · JULY 2012

Impact Factor: 4.77 · DOI: 10.1021/jp303226u

THE JOURNAL OF PHYSICAL CHEMISTRY C

Article

pubs.acs.org/JPCC

Magnetoresistive Conductive Polyaniline–Barium Titanate Nanocomposites with Negative Permittivity

Xi Zhang,[†] Suying Wei,*[,‡] Neel Haldolaarachchige,[§] Henry A. Colorado,[∥] Zhiping Luo,[⊥] David P. Young,[§] and Zhanhu Guo*[,†]

[†]Integrated Composites Laboratory (ICL), Dan F. Smith Department of Chemical Engineering, and [‡]Department of Chemistry and Biochemistry, Lamar University, Beaumont, Texas 77710, United States

[§]Department of Physics and Astronomy, Louisiana State University, Baton Rouge, Louisiana 70803, United States

[∥]Department of Materials Science and Engineering, University of California Los Angeles, Los Angeles, California 90095, United States

[⊥]Department of Chemistry and Physics, Fayetteville State University, Fayetteville, North Carolina 28301, United States

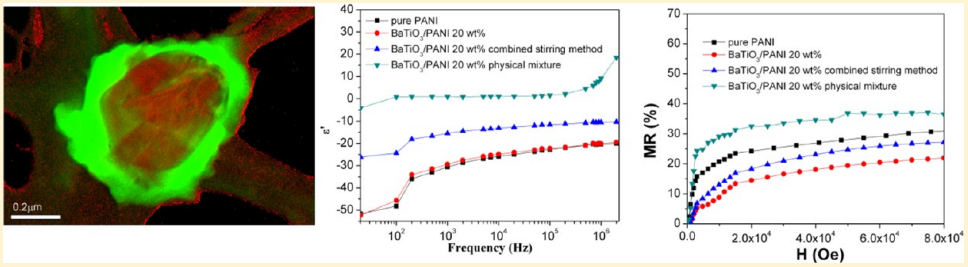

ABSTRACT: Polyaniline (PANI) polymer nanocomposites (PNCs) filled with barium titanate ($BaTiO_3$) were synthesized by a surface initiated polymerization method. Two different particle sizes (100 and 500 nm) were studied. By varying the loading level, size of $BaTiO_3$ nanoparticles (NPs) and stirring method for the polymerization process, a series of PNCs were obtained and the effects of these parameters on the crystalline structure, thermal stability, morphology, electrical conductivity and dielectric permittivity were systematically studied. FT-IR analysis indicated a strong interaction between the formed PANI and the $BaTiO_3$ NPs, and TEM observations showed that the $BaTiO_3$ NPs are well coated with a PANI layer, however, the thickness of the PANI layer decreased with increasing the $BaTiO_3$ particles loading. The XRD reflection patterns indicated that the crystallinity of the polyaniline part in the PNCs depends on the nanoparticle loading. However, the resistivity does not increase with increasing the crystallinity, and the temperature dependent resistivity result reveals a 3-d variable range hopping (VRH) electron transport mechanism. The $BaTiO_3$ loading dependent resistivity is interpreted from the dominating space charge on the $BaTiO_3$/PANI interface and the ferroelectric nature of $BaTiO_3$ for the PNCs with different particle loadings. Compared with the positive real permittivity for the PNCs prepared from physical mixing, all the chemically synthesized PNC samples show negative dielectric permittivity and the permittivity change is related to the instinct metallic state in PANI. In addition, positive magnetoresistance (MR) is observed in all kinds of PNCs and analyzed theoretically from the wave function shrinkage model.

1. INTRODUCTION

Polymer nanocomposites (PNCs) have attracted more attention due to their wide potential applications[1−3] arising from their unique electrochemical, mechanical and magnetic properties.[4,5] Among the PNCs, conductive PNCs are one of the most important materials. Generally, two broad categories are classified. One is adding conductive nanofillers to the insulating polymer matrix, and the other is to use the conductive polymer as the hosting matrix. The introduction of nanoparticles (NPs) can improve the properties of polymers such as thermal stability,[6] magnetic property[7] and dielectric switching frequency.[8] In addition, compared to the traditional composites, conductive PNCs have great potential applications[9] such as magnetic field sensors,[10] energy electrodes[11] and biosensors.[12,13]

Barium titanate ($BaTiO_3$) as transition metal oxides exhibits unique properties including ferroelectricity,[14] piezoelectricity[15] and high dielectric constant[16] and has been used to improve the dielectric property of the polymers. For example, polyvinylidene fluoride (PVDF) or siloxane-modified polyamideimide (SPAI) filled with $BaTiO_3$ has been used to prepare high dielectric thin films.[17] And nanosized $BaTiO_3$ dispersed in polyvinylpyrrolidone (PVP) and quaternary acrylic resin (RMX) can be applied as high capacitance films[18] and humidity sensors,[19] respectively. However, due to the poor binding between inorganic fillers and the organic matrix, surface modifications are normally required to improve the dispersibility of $BaTiO_3$ in polymer matrix. For instance, core–shell $BaTiO_3$-polystyrene-block-poly(styrene-*co*-vinylbenzylchloride) (PS-*b*-PSVBC) is prepared to ensure a better dispersibility in

Received: April 4, 2012
Revised: June 24, 2012
Published: July 5, 2012

nonpolar polymer matrix.[20] Polyaniline (PANI) as a conjugated polymer attracts more attention owing to its controllable doping levels[21−23] and wide range of applications such as anticorrosion coating,[24] sensors,[25] reduction of toxic Cr(VI) in water[26] and tissue engineering.[27] In addition, compared with bulk form, PANI nanostructures have larger interfacial area,[28,29] which improves the dispersibility in the hosting matrix. Due to the outstanding advantages, PANI has been widely applied in conductive PNCs to form the conductive layer and improve the conductivity,[7] stability and dipersibility of the nanoparticles.[30]

The $BaTiO_3$/PANI PNCs synthesized by *in situ* polymerization with mechanical stirring, combining the unique dielectric property of $BaTiO_3$ and conductive properties of PANI together, have shown great applications. For example, with a high reflection loss of −15 dB at high frequency (10 GHz), the $BaTiO_3$−PANI composites have been applied in microwave absorption field, and the absorption property is observed to be enhanced with increasing the weight percentage of PANI.[31] In addition, $BaTiO_3$/PANI can be used as electrorheological (ER) materials; at 3.5 kV/mm the shear stress of the $BaTiO_3$/PANI (20 vol %) in silicone oil reaches 2800 Pa, which is higher than that of pure PANI in silicone oil and pure $BaTiO_3$ in silicone oil.[32] However, research on $BaTiO_3$/PANI is mainly focused on the ER phenomenon; there is limited discussion on the electron transport mechanism of the $BaTiO_3$/PANI PNCs, and the magnetoresistance is rarely reported in the literature. Although there is a report on the dielectric permittivity decreasing sharply with increasing the PANI loading,[33] the value is still above zero.

Giant magnetoresistance (GMR), defined as a large change in resistance when the relative orientation of the magnetic domains in adjacent layers is adjusted from antiparallel to parallel under an applied magnetic field, was first discovered in alternating ferromagnetic iron and nonferromagnetic chromium layers.[34] Not only does the metal material possess the GMR but also a huge resistance change with an applied external magnetic field was observed in organic materials, and termed as organic magnetoresistance (OMR). OMR is generally observed in π-conjugated materials and is believed to originate from the spin correlations among the interacting charge carriers. Various polarons are considered to explain the OMR, such as in the electron−hole (e−h) pair model,[35] the anomalous MR in the semiconductor is related to the limitation of the recombination of the electrons and holes; and the bipolaron model[36] with the effects of electron and hole being studied separately can be used to explain the transition between positive and negative MR. A good understanding of the mechanism of MR will be beneficial to the applications of these organic semiconductors.[37] In addition, due to the tunable electronic property and easy processability, π-conjugated organic semiconductors have significant technological applications such as information display and large-area electronics.[38] Owing to the unique negative physical properties such as refractive index and permittivity, metamaterials have attracted great interest. Recently, negative permittivity was discovered by our group in conductive polymer-based nanocomposites (PNCs) such as polyaniline−tungsten oxide, polypyrrole−tungsten oxide,[8,9] polypyrrole−carbon nanostructures[39,40] and elastomer/carbon nanofiber (CNF) PNCs.[41] These materials obtain a promising future that can be applied in cloaking, superlens, wave filters, remote aerospace engineering and superconductors.[42−44] However, MR and negative permittivity, especially with a combined MR and negative properties in the PNCs, have been rarely reported.

In this paper, $BaTiO_3$/PANI PNCs are synthesized by a surface initiated polymerization (SIP) method with both ultrasonication and mechanical stirring. By varying the $BaTiO_3$ nanoparticle loading level, dispersion methods and $BaTiO_3$ nanoparticle size in the PNCs, a series of PNCs are obtained and studied. A sample physical mixing of PANI and $BaTiO_3$ nanoparticles is also used to prepare one nanocomposite sample for property comparison. The morphology, crystallinity, dielectric permittivity and thermal stability of the obtained $BaTiO_3$/PANI PNCs are investigated and compared with each other. Electron transport mechanism is explored by researching the temperature dependent resistivity. Unique dielectric property and OMR are observed in the PNCs and are analyzed theoretically.

2. EXPERIMENTAL SECTION

2.1. Materials. Aniline (C_6H_7N), ammonium persulfate (APS, $(NH_4)_2S_2O_8$) and *p*-toluene sulfonic acid (PTSA, $C_7H_8O_3S$) were all purchased from Sigma Aldrich. Barium titanate ($BaTiO_3$) (500 and 100 nm) was purchased from Nanostructure & Amorphous Materials Inc. All the chemicals were used as-received without any further treatment.

2.2. Preparation of $BaTiO_3$/PANI Nanocomposites. *2.2.1. $BaTiO_3$/PANI Nanocomposites.* The molar ratio used in this method was aniline:APS:PTSA = 6:3:5.[45] For solution one, PTSA (60 mM) and APS (36 mM) and $BaTiO_3$ NPs were dissolved in deionized water (400 mL), and then the solution was put in an ice−water bath and under ultrasonication for one hour. Solution two was aniline (72 mM) dissolved in deionized water (100 mL). Then solution two was added into solution one and the mixture was sonicated for an additional one hour in an ice−water bath for polymerization. Finally, the product was vacuum filtered and washed with ethanol and deionized water to remove excess acid, any possible oligomers and organic solvent. Then the obtained powders were dried completely at 50 °C. The PNCs with a $BaTiO_3$ (500 nm) particle loading of 1.0, 5.0, 10.0 and 20.0 wt % were prepared. Pure PANI was synthesized following the same procedures without adding any $BaTiO_3$ NPs for comparison.

The $BaTiO_3$/PANI PNCs prepared by simple physical mixing with a loading of 20.0 wt % were also fabricated to illustrate the coating effect. The $BaTiO_3$/PANI PNCs with a loading of 20.0 wt % prepared by a combined stirring method (ultrsonication and mechanical stirring) were also prepared to see whether the stirring methods have a certain influence on the coating process.

The $BaTiO_3$(100 nm)/PANI PNCs with a particle loading of 1.0, 5.0, 10.0 and 20.0 wt % were also synthesized by combined stirring methods to study the effect of nanoparticle size on the physical properties of the obtained PNCs.

2.3. Characterization. *2.3.1. Fourier Transform Infrared Spectroscopy (FT-IR).* The FT-IR (Bruker Inc. Vector 22, coupled with an ATR accessory) was used to characterize pure PANI and the $BaTiO_3$/PANI PNCs in the range of 500 to 4000 cm^{-1} at a resolution of 4 cm^{-1}. FT-IR was also used to determine the nanoparticle surface functionality.

2.3.2. Morphological Characterizations of the $BaTiO_3$/PANI Nanocomposites. The morphology of the $BaTiO_3$/PANI nanostructures was characterized with a scanning electron microscope (SEM, JEOL field emission scanning electron microscope, JSM-6700F). The structures of the PNCs were

further characterized by transmission electron microscopy (TEM) using a FEI Tecnai G^2 F20 with a field emission gun, operated at an accelerating voltage of 200 kV. The TEM samples were prepared by drying a drop of the ethanol suspension on carbon-coated copper TEM grids.

2.3.3. Crystalline Structure of $BaTiO_3$/PANI PNCs. The crystalline structure of the $BaTiO_3$/PANI PNCs was studied by X-ray diffraction (XRD), which was accomplished in a Bruker D8 Focus diffractometer equipped with a Sol-X detector using a copper radiation source. Data were collected in the range of 2θ = 5−75° at a resolution of 0.05° per step with a 6 s integration time per step.

2.3.4. Thermal Characterization of $BaTiO_3$/PANI PNCs. The thermal stability of the $BaTiO_3$/PANI PNCs was studied by a thermogravimetric analysis (TGA, TA Instruments Q-500). All the $BaTiO_3$/PANI samples were heated from 30 to 700 °C with an air flow rate of 60 mL/min and a heating rate of 20 °C/min.

2.3.5. Resistivity, Dielectric Permittivity and Magnetoresistance Measurement. The samples of pure PANI and the $BaTiO_3$/PANI PNCs were pressed in the form of disk pellets with a diameter of 25 mm by applying a pressure of 95 MPa in a hydraulic presser, and the average thickness was about 0.5 mm. The electrical resistivity was measured following a standard four probe method in the temperature range of 100−290 K. The temperature dependent resistivity was used to investigate the electron transport mechanism in the $BaTiO_3$/PANI PNC samples. The magnetic field dependent resistance was carried out using a standard four-probe technique by using the same samples. The dielectric permittivity was measured by a LCR meter (Agilent, E 4980A) equipped with a dielectric test fixture (Agilent, 16451B) at the frequency of 20−2 × 10^6 Hz. A piece of rectangular standard Teflon sample with a permittivity of 2.1−2.4 is used for calibration before the test.

3. RESULTS AND DISCUSSION

3.1. FT-IR Analysis. Figure 1 shows the FT-IR spectra of pure PANI, pure $BaTiO_3$ and the $BaTiO_3$/PANI PNCs with different loadings of $BaTiO_3$ NPs. Pure PANI shows peaks at 1560, 1483 and 1294 cm^{-1} corresponding to the stretching

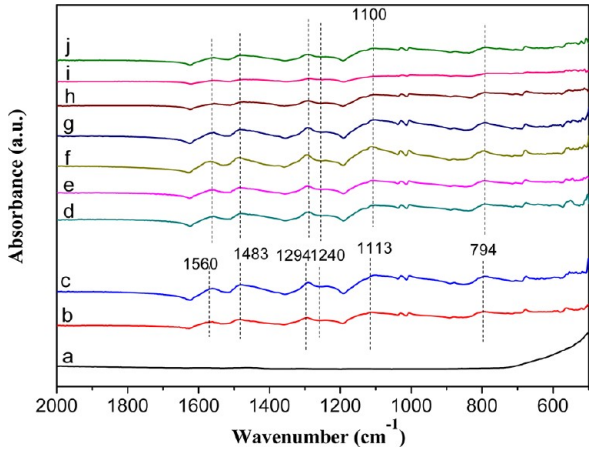

Figure 1. FT-IR spectra of (a) pure $BaTiO_3$; (b) pure PANI; (c) $BaTiO_3$/PANI PNCs prepared by physical mixture; $BaTiO_3$(500 nm)/PANI PNCs with a $BaTiO_3$ loading of (d) 1 wt %, (e) 5 wt %, (f) 10 wt % and (g) 20 wt %; (h) $BaTiO_3$(500 nm)/PANI PNCs with a $BaTiO_3$ loading of 20 wt % prepared by combined stirring method; (i) $BaTiO_3$(100 nm)/PANI PNCs with a $BaTiO_3$ loading of 1 wt %; and (j) $BaTiO_3$(100 nm)/PANI PNCs with a $BaTiO_3$ loading of 20 wt %.

deformation of quinone, benzene rings and C−N of aromatic amine of PANI, respectively.[8] Peaks at 1240 and 1113 cm^{-1} are attributed to the C−H stretch and C−N stretch in the quinoid ring, respectively.[45] The peak at 794 cm^{-1} indicates the out-of-plane bending of C−H in the substituted benzene ring.[45] From Figure 1, peaks belonging to PANI can also be observed in the PNCs, indicating the formation of PANI. When PNCs prepared with different methods were compared, for the physical mixed sample (Figure1c), no peak shift was observed when compared with pure PANI; however, peaks of the PNCs prepared by chemically synthesized method shift to lower wavenumbers. For example, the peak of C−N stretch in the quinoid ring shifts from 1113 cm^{-1} for pure PANI, Figure 1a, to 1110 cm^{-1} for the $BaTiO_3$(500 nm)/PANI PNCs with a loading of $BaTiO_3$ 10 wt %, Figure 1f, and further to 1100 cm^{-1} for $BaTiO_3$(500 nm)/PANI PNCs with a loading of $BaTiO_3$ 20 wt %, Figure 1g, respectively. The peak shift demonstrates a strong interaction between PANI and $BaTiO_3$, which is associated with the localization effect.[8]

3.2. Morphology of $BaTiO_3$/PANI PNCs. Figure 2 shows the SEM microstructures of pure PANI, pure $BaTiO_3$(500 nm) and the $BaTiO_3$/PANI PNCs with various weight loadings of $BaTiO_3$. Pure PANI particles are observed to have a rough surface with a smaller size; however, the $BaTiO_3$ particles are observed to have a larger size, and the surface is fairly smooth. These obvious differences of size and surface are applied to distinguish $BaTiO_3$ and PANI in the study of PNCs samples. For the $BaTiO_3$/PANI PNCs, when the weight percentage of $BaTiO_3$ is lower such as 1.0 wt %, Figure 2c, and 5.0 wt %, Figure 2d, no bare $BaTiO_3$ particles are observed in the SEM image, indicating that the $BaTiO_3$ particles are well coated with PANI. The same phenomenon is also observed from the TEM image. Figure 3 shows the TEM microstructures of the $BaTiO_3$/PANI PNCs. For the $BaTiO_3$(500 nm)/PANI PNCs with 1 wt % loading, Figure 3a, $BaTiO_3$ NPs are well coated with PANI and the PANI layer is fairly thick. In the $BaTiO_3$(500 nm)/PANI PNCs with a loading of 5 wt %, Figure 3b, the PANI layer becomes thinner than that of the coating in the $BaTiO_3$(500 nm)/PANI PNCs with a loading of 1 wt %, Figure 3a. However, the $BaTiO_3$ particles are still well coated with a PANI layer.

In Figure 2, when the loading of $BaTiO_3$(500 nm) is further increased to higher loading (10 wt % and 20 wt %), $BaTiO_3$ particle exposed to surrounding without coating of PANI can be found in SEM images. Obvious $BaTiO_3$ particle can be observed in $BaTiO_3$(500 nm)/PANI with loading of $BaTiO_3$ 10 wt %, Figure 2e, samples; and when the loading increased to 20 wt %, Figure 2f, more $BaTiO_3$ particles can be observed, and the particles tend to agglomerate together. The same tendency can be also obtained from the TEM photo, in $BaTiO_3$(500 nm)/PANI with a loading of $BaTiO_3$ 10 wt % samples, Figure 3c, some $BaTiO_3$ particles are only partly coated with PANI, and in $BaTiO_3$(500 nm)/PANI PNCs with a $BaTiO_3$ loading of 20 wt % samples, Figure 3d, some $BaTiO_3$ particles look like they are completely uncovered. The variation in coating situation is related to the polymerization mechanism. The coating process was previously studied in our group and explored by surface initiated polymerization (SIP);[45] it is proved that the NPs are covered by acid and oxidant after the ultrasonication treatment, and with the addition of monomer, the polymerization will take place on the surface of NPs, which means that the polymer chains will grow on the NPs and surround them.[45] In the PNCs with lower $BaTiO_3$(500 nm)

dx.doi.org/10.1021/jp303226u | J. Phys. Chem. C 2012, 116, 15731−15740

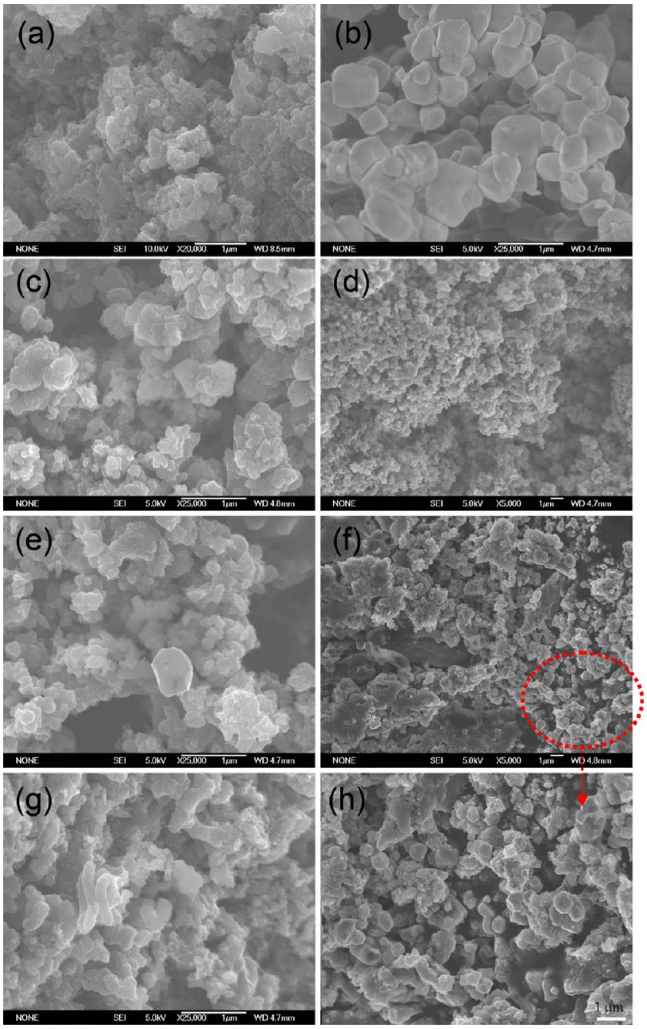

Figure 2. SEM microstructures of (a) pure PANI; (b) pure $BaTiO_3$(500 nm); $BaTiO_3$(500 nm)/PANI PNCs with a $BaTiO_3$ loading of (c) 1 wt %, (d) 5 wt %, (e) 10 wt %, (f) 20 wt %; (g) $BaTiO_3$(500 nm)/PANI with a $BaTiO_3$ loading of 20 wt % prepared by combined stirring methods, (h) enlarged part of $BaTiO_3$(500 nm)/PANI with a $BaTiO_3$ loading of 20 wt %.

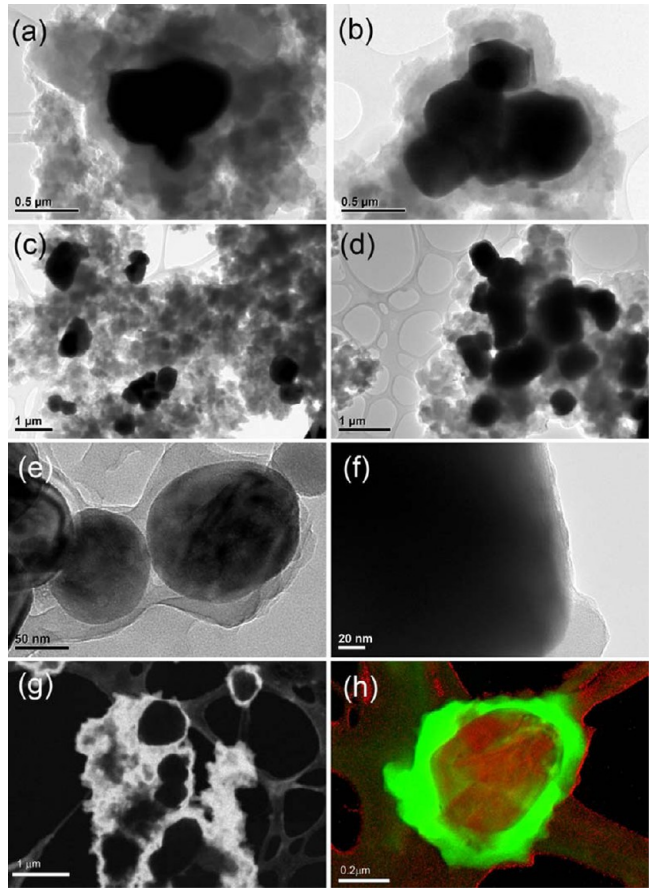

Figure 3. TEM microstructures of $BaTiO_3$(500 nm)/PANI PNCs with a $BaTiO_3$ loading of (a) 1 wt %, (b) 5 wt %, (c) 10 wt % and (d) 20 wt %; (e) $BaTiO_3$(100 nm)/PANI with a $BaTiO_3$ loading of 20 wt %; (f) $BaTiO_3$(500 nm)/PANI with $BaTiO_3$ loading of 20 wt %, (g) $BaTiO_3$(500 nm)/PANI with $BaTiO_3$ loading of 20 wt % prepared by combined stirring methods, (h) energy-filtered TEM of $BaTiO_3$(500 nm)/PANI with $BaTiO_3$ loading of 20 wt % prepared by combined stirring methods.

loadings, for example, 1 wt %, Figure 3a, and 5 wt %, Figure 3b, there are limited NPs and the amount of acid and oxidant is larger, thus a thicker PANI layer is formed on the surface of $BaTiO_3$ particles; however, the total surface area of NPs will increased with increasing $BaTiO_3$ loading, and thus, the PANI layer becomes thinner. In the PNCs with higher $BaTiO_3$(500 nm) loadings, for example, 10 wt %, Figure 3c, and 20 wt %, Figure 3d, the surface area of NPs is sharply enlarged, and limited acid, oxidant and monomer are not sufficient to grow a thick PANI coating, which is observed in the SEM photo where it appears that the PANI layer is unable to coat the whole surface of $BaTiO_3$ particles. However, when the surface of $BaTiO_3$ particles is studied in detail in TEM, Figure 3f, a pretty thin layer of PANI coating is distinguishable on the surface of particles. Thus, when the $BaTiO_3$ particle loading increased, the thickness of the PANI layer is decreased, but it can still form a layer to cover the surface of $BaTiO_3$ particles.

Comparing $BaTiO_3$/PANI PNCs prepared with different methods, in $BaTiO_3$(500 nm)/PANI PNCs with a $BaTiO_3$ loading of 20 wt % samples prepared by combined stirring methods from both SEM, Figure 2g, and TEM, Figure 3g, no obvious $BaTiO_3$ particles can be observed, and in SEM image some fiber shape PANI is formed. In TEM image, different with $BaTiO_3$(500 nm)/PANI with a $BaTiO_3$ loading of 20 wt % sample prepared just by ultrasonication, Figure 3f, in $BaTiO_3$(500 nm)/PANI with loading of $BaTiO_3$ 20 wt % samples prepared by combined stirring methods, although the PANI layer is much thinner than for samples with lower loading of $BaTiO_3$ nanoparticles, the $BaTiO_3$ particles are still well coated with PANI. Energy-filtered TEM (EFTEM) is applied on the $BaTiO_3$(500 nm)/PANI PNCs with a $BaTiO_3$ loading of 20 wt % prepared by combined stirring methods, Figure 3h, to clarify the outside (coating layer) and inside (particle) component; the green part represents the PANI layer, and the red part represents the Ti element. EFTEM reveals that the $BaTiO_3$ particles are well coated by the PANI layer. Thus, the interaction of ultrasonication and mechanical stirring is beneficial for the polymer chains to grow on the surface of NPs.

The morphology of PNCs prepared with different size of $BaTiO_3$ NPs is also compared. For 100 nm $BaTiO_3$ NPs, with increasing $BaTiO_3$ loading, Figure 4a–d, more $BaTiO_3$ particles can be observed, which follows the same tendency obtained from prior discussion. However, different from PNCs prepared with large size (500 nm), $BaTiO_3$ particles (100 nm) without coating can be observed even in the 1 wt % samples, Figure 4a,

dx.doi.org/10.1021/jp303226u | J. Phys. Chem. C 2012, 116, 15731–15740

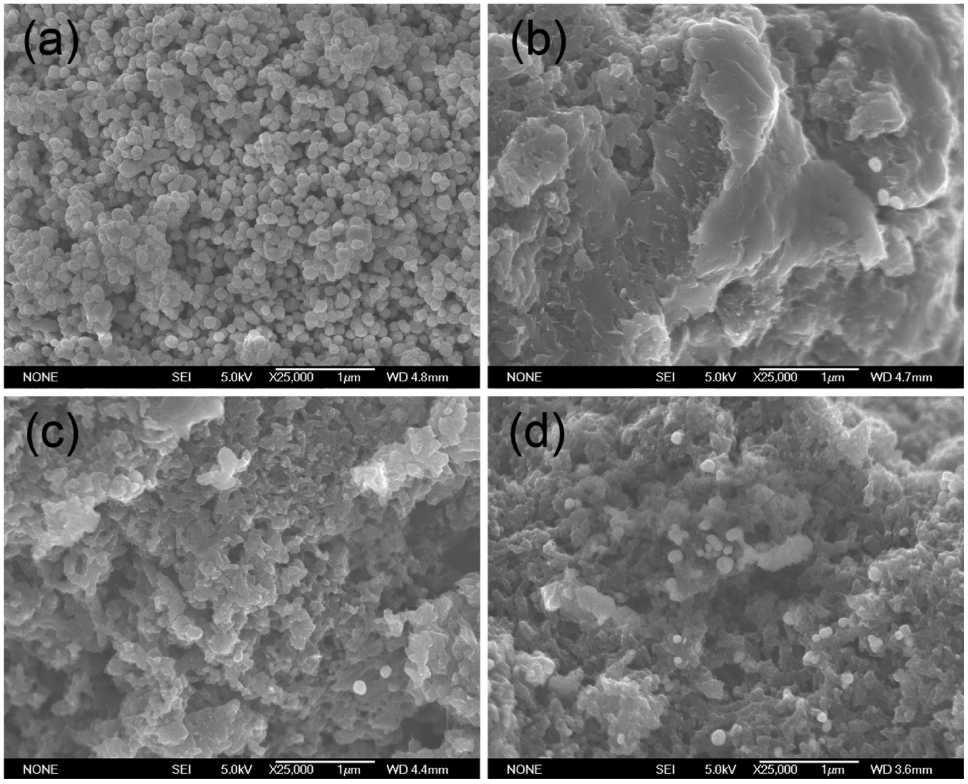

Figure 4. SEM microstructures of $BaTiO_3$/PANI PNCs prepared with a $BaTiO_3$ particle (100 nm) loading of (a) 1 wt %, (b) 5 wt %, (c) 10 wt % and (d) 20 wt %.

indicating that the polymer chains become harder to grow on it with decreasing particle size. This may attributed to the greater surface area of $BaTiO_3$ NPs with smaller size. However, when the structure of PNCs is studied by TEM, a thinner PANI layer is also observed in $BaTiO_3$(100 nm)/PANI PNCs with a $BaTiO_3$ loading of 20 wt %, Figure 3e, as discussed previously in PNCs with $BaTiO_3$ of 500 nm.

3.3. X-ray Diffraction. Figure 5 shows the XRD patterns of the pure PANI, pure $BaTiO_3$ and the $BaTiO_3$/PANI PNCs with different $BaTiO_3$ weight loading. The peaks with 2θ at 22.35, 31.55, 38.95,45.40, 51.00, 56.20 and 65.80° correspond to the (100), (110), (111), (200), (210), (211) and (220) plane of $BaTiO_3$.[33] The relatively broad peaks at 2θ equal to 15.75, 20.25 and 25.15° represent the (100), (110) and (111) planes of PANI.[46] The crystallinity of the PANI nanostructures is calculated by TOPAS software and is obtained as the crystalline area divided by the sum of crystalline area and amorphous area. The result shows that the crystallinity of PANI increases from 7.48 to 11.06% for pure PANI, Figure 5Aa, and $BaTiO_3$(500 nm)/PANI PNCs with a $BaTiO_3$ loading of 1 wt %, Figure 5Ab, respectively. The increment of crystallinity can be explained by the heterogeneous nucleation process of the polymers. Specifically, $BaTiO_3$ nanoparticles introduced in the monomer solution act as "nucleating sites" for the growth of the PANI chain and improve the crystalline process of PANI.[45] However, with further increase in the loading of $BaTiO_3$ NPs, the degree of crystallinity is reduced to 3.18% for $BaTiO_3$(500 nm)/PANI PNCs with a $BaTiO_3$ loading of 5 wt %, which is attributed to the enlarged size of $BaTiO_3$ NPs. With the amount of NPs increased, the formed larger aggregates of the agglomerated NPs will hinder the growth of polymer chains.[47] For peaks in the PNCs attributed to the $BaTiO_3$ nanoparticles, no shift is observed with increasing the $BaTiO_3$ loading, however, the intensity of peaks keeps enlarging and reaches almost the same value of pure $BaTiO_3$ at $BaTiO_3$(500 nm)/PANI PNCs with a $BaTiO_3$ loading of 20 wt %, Figure 5B. The weakened peak is due to the growth of polymer chains on the surface of $BaTiO_3$ NPs, which impedes the detection function of X-rays on the inorganic NPs.

Comparing the $BaTiO_3$(500 nm)/PANI PNCs with a $BaTiO_3$ loading of 20 wt %, Figure 5Ca, $BaTiO_3$(500 nm)/PANI PNCs with a $BaTiO_3$ loading of 20 wt % prepared by simple physical mix method, Figure 5Cb, and $BaTiO_3$(500 nm)/PANI PNCs with a $BaTiO_3$ loading of 20 wt % prepared by a combined stirring method, Figure 5Cc, peaks of (200), (210), (211), (220) planes of $BaTiO_3$ shift to the lower degree side in the $BaTiO_3$(500 nm)/PANI PNCs with a $BaTiO_3$ loading of 20 wt % physical mixture, Figure 5Cb sample. For crystalline materials, the lattice plane d-spacing is calculated based on the Bragg formula,[48] eq 1:

$$\lambda = 2d \sin\theta \quad (1)$$

where λ is the X-ray wavelength (λ = 1.5406 Å) and θ is the diffraction angle. When the value of θ shifts to lower angle, the d-spacing will increase, which means that the PNCs prepared by physically mixing $BaTiO_3$ and PANI will increase the lattice plane of $BaTiO_3$. No obvious peak shift or intensity change is observed between the $BaTiO_3$(500 nm)/PANI PNCs with a $BaTiO_3$ loading of 20 wt %, Figure 5Ca, and the $BaTiO_3$(500 nm)/PANI PNCs with a $BaTiO_3$ loading of 20 wt % prepared by a combined stirring method, Figure 5Cc, indicating that the variation of mixing method has no influence on the crystalline structure of the PNCs.

Similarly, comparing the crystalline structure of the $BaTiO_3$(100 nm)/PANI PNCs, Figure 5Bc,g, and $BaTiO_3$(500 nm)/PANI PNCs, Figure 5Bb,d–f, no peak shift

dx.doi.org/10.1021/jp303226u | J. Phys. Chem. C 2012, 116, 15731–15740

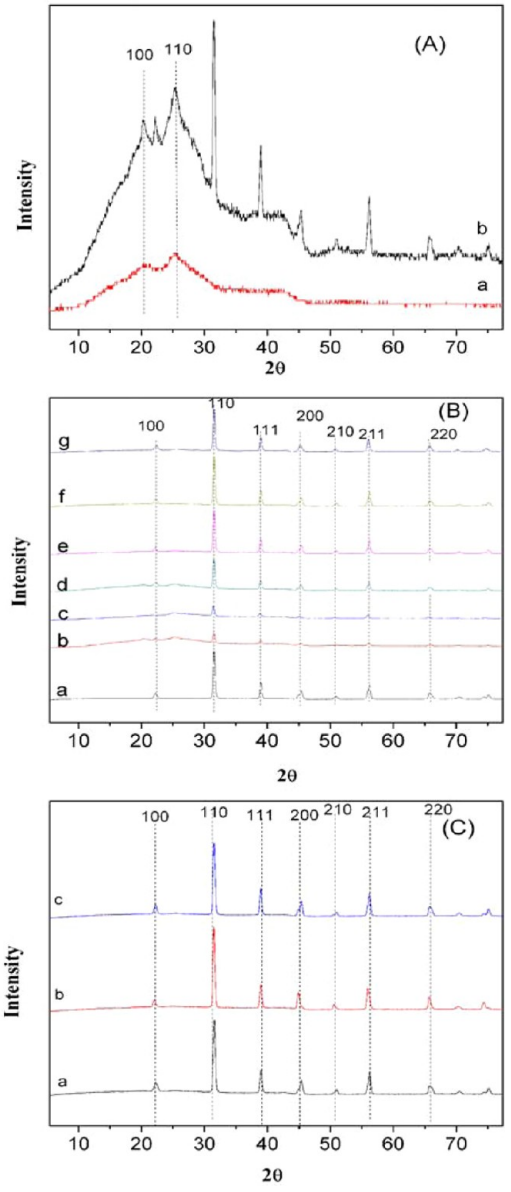

Figure 5. X-ray diffraction patterns of the (A) (a) pure PANI, (b) $BaTiO_3$(500 nm)/PANI PNCs with a $BaTiO_3$ loading of 1 wt %; (B) (a) pure $BaTiO_3$(500 nm), (b) $BaTiO_3$(500 nm)/PANI PNCs with a $BaTiO_3$ loading of 1 wt %, (c) $BaTiO_3$(100 nm)/PANI with a $BaTiO_3$ loading of 1 wt %, (d) $BaTiO_3$(500 nm)/PANI with a $BaTiO_3$ loading of 5 wt %, (e) $BaTiO_3$(500 nm)/PANI with a $BaTiO_3$ loading of 10 wt %, (f) $BaTiO_3$(500 nm)/PANI PNCs with a $BaTiO_3$ loading of 20 wt %, (g) $BaTiO_3$(100 nm)/PANI with a $BaTiO_3$ loading of 20 wt %; (C) (a) $BaTiO_3$(500 nm)/PANI with a $BaTiO_3$ loading of PNCs 20 wt %, (b) $BaTiO_3$(500 nm)/PANI PNCs with $BaTiO_3$ loading of 20.0 wt % physical mixture, (c) $BaTiO_3$(500 nm)/PANI with a $BaTiO_3$ loading of 20 wt % prepared with combined stirring mixture.

or intensity enhancement is observed, thus, the crystalline structure of $BaTiO_3$/PANI PNCs is not depending on the size of the $BaTiO_3$ NPs.

3.4. Thermogravimetric Analysis. Figure 6 shows the TGA curves of the PNCs with different loadings of $BaTiO_3$. The first weight loss stage from room temperature to 150 °C is attributed to the release of the moisture and the residue organic solvent entangled in the polymer chains. With temperature increased, a slight weight loss stage is observed at around 250 °C, which is due to the loss of the doped acid in PANI.[49,50] At

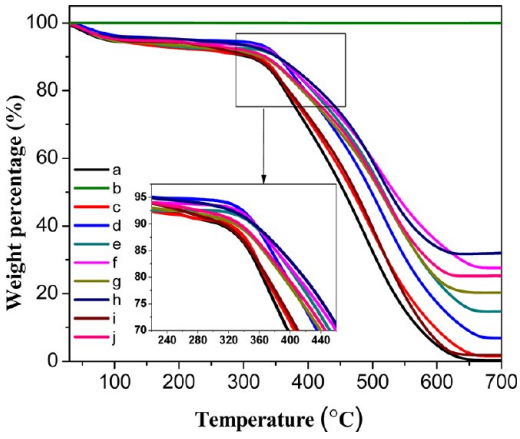

Figure 6. TGA curves of (a) pure PANI; (b) pure $BaTiO_3$(500 nm); $BaTiO_3$(500 nm)/PANI PNCs with a $BaTiO_3$ loading of (c) 1 wt %, (d) 5 wt %, (e) 10 wt % and (f) 20 wt %; (g) $BaTiO_3$(500 nm)/PANI PNCs with a $BaTiO_3$ loading of 20 wt % by physical mixture; (h) $BaTiO_3$(500 nm)/PANI PNCs with a $BaTiO_3$ loading of 20 wt % prepared by combined stirring mixture; and $BaTiO_3$(100 nm)/PANI PNCs with a $BaTiO_3$ loading of (i) 1 wt % and (j) 20 wt %.

above 300 °C, the third weight loss stage related to the degradation of PANI is observed. Table 1 summarizes the onset

Table 1. Onset Decomposition Temperature and Weight Loss for Pure PANI and $BaTiO_3$/PANI PNCs

samples	onset temp (°C) second wt loss stage	onset temp (°C) third wt loss stage	wt (%) in 700 °C
pure PANI	213.56	335.18	0.00
$BaTiO_3$(500 nm)/PANI			
with $BaTiO_3$ loading of 1.0 wt %	250.80	335.05	1.98
with $BaTiO_3$ loading of 5.0 wt %	230.97	338.56	6.97
with $BaTiO_3$ loading of 10.0 wt %	209.63	344.07	21.85
with $BaTiO_3$ loading of 20.0 wt %	210.38	347.41	28.05
with $BaTiO_3$ loading of 20.0 wt % physical mixture	240.72	293.62	20.59
with $BaTiO_3$ loading of 20.0 wt % prepared by combined stirring methods	209.74	352.94	32.00
$BaTiO_3$(100 nm)/PANI			
with $BaTiO_3$ loading of 1.0 wt %	221.56	330.93	2.39
with $BaTiO_3$ loading of 5.0 wt %	224.32	337.09	9.17
with $BaTiO_3$ loading of 10.0 wt %	211.99	349.95	16.89
with $BaTiO_3$ loading of 20.0 wt %	217.69	349.22	25.58

temperatures of the second and third weight loss stages of the PNCs. The onset decomposition temperature for the second weight loss stage sharply increases in the PNCs with lower particle loading (1 wt %), and begins to decrease in the PNCs with the particle loading of 5 wt %. The degradation temperature variation is related to the crystallinity of PANI in the PNCs. From the study of crystalline structure of the PNCs, the crystallinity of PANI in the PNCs with lower $BaTiO_3$ particle loadings (1 wt %) is increased to 11.06%; however, with the loading of $BaTiO_3$ increased, the crystallinity is decreased (3.18% for the PNCs with a $BaTiO_3$ loading of 5 wt %). For the third weight loss stage, the onset decomposition temperature keeps increasing with increasing $BaTiO_3$ loading and the enhanced decomposition temperature is associated

dx.doi.org/10.1021/jp303226u | J. Phys. Chem. C 2012, 116, 15731−15740

with the stronger chemical interaction between PANI and $BaTiO_3$.[51] For $BaTiO_3$(500 nm)/PANI PNCs with a $BaTiO_3$ loading of 1 wt %, only a limited amount of polymer chains is grown on the nanoparticle surface and majority of polymer chains are present in the bulk form, which causes slightly increased decomposition temperature in the third weight loss stage compared to that of pure PANI. However, for the $BaTiO_3$(500 nm)/PANI PNCs with a $BaTiO_3$ loading of 10 wt %, Figure 6e, due to the enlarged surface area between PANI and $BaTiO_3$, the interaction is greatly increased and thus more energy is required to destroy the PNC structure, which causes a largely increased onset decomposition temperature.

The PNC sample prepared by simple physical mixing, Figure 6g, has lower decomposition temperature than the chemically synthesized sample with the same composition, Figure 6f, demonstrating that an improved thermal stability is due to stronger interaction between PANI and $BaTiO_3$. The TGA result has also demonstrated the same phenomenon, the PNCs prepared with a combined stirring method, Figure 6h, have higher onset decomposition temperature than the sample prepared with only ultrasonication, Figure 6f, which indicates a better interaction between PANI and $BaTiO_3$ in the PNCs. Comparing the thermal stability of the PNCs prepared with different $BaTiO_3$ particle size, the PNCs with smaller size (100 nm) have lower onset temperature of decomposition process, Table 1. In addition, the residual of the PNCs at 700 °C is $BaTiO_3$ only with PANI being completely decomposed in air and at such a high temperature, Figure 6a. From Table 1, the weight percentage of the residual is lower than that estimated from the initial reactants, which is attributed to the incomplete polymerization of monomers.[45] During the experiment, it is observed that, compared with pure PANI, the time needed for the formation of PANI in PNCs is longer, which also demonstrates that the conversion of monomers to PANI is affected by the introduced $BaTiO_3$ NPs.

3.5. Electrical Conductivity (σ). Figure 7A shows the resistivity as a function of temperature for pure PANI and the $BaTiO_3$/PANI PNCs. The electron transport mechanism is investigated by exploring the relationship between temperature and σ using eq 2:[8,51]

$$\sigma = \sigma_0 \exp\left[-\left(\frac{T_0}{T}\right)^{1/n}\right] \quad (2)$$

where T_0 is the characteristic Mott temperature related to the electronic wave function localization degree, σ_0 is the conductivity at infinite high temperature and n can be equal to 2, 3 and 4, which represent one-, two- and three-dimensional systems, respectively. Here n is equal to 4, which is the best fit for each sample, Figure 7B, indicating a 3-d VRH behavior. The obtained T_0 and σ_0 values for each sample are summarized in Table 2. In the whole temperature range, first, the resistivity increases when the loading of $BaTiO_3$(500 nm) increases from 0.0 to 10 wt %, Figure 7Aa–d; however, when the loading of $BaTiO_3$(500 nm) increased to 20 wt %, Figure 7Ae, the resistivity decreased sharply. For the $BaTiO_3$/PANI PNCs when adding an external voltage, the charge dissipated in the PNCs can result from the ferroelectric nature of $BaTiO_3$ and also attributed tohat the space charge at the interface between $BaTiO_3$ and PANI.[52] Although at lower loading, for example, 1.0 wt %, the adding of $BaTiO_3$ particles increases the crystallinity of PANI, the charge transport is limited. In Table 2 with increasing loading of $BaTiO_3$(500 nm) particles from 0 to

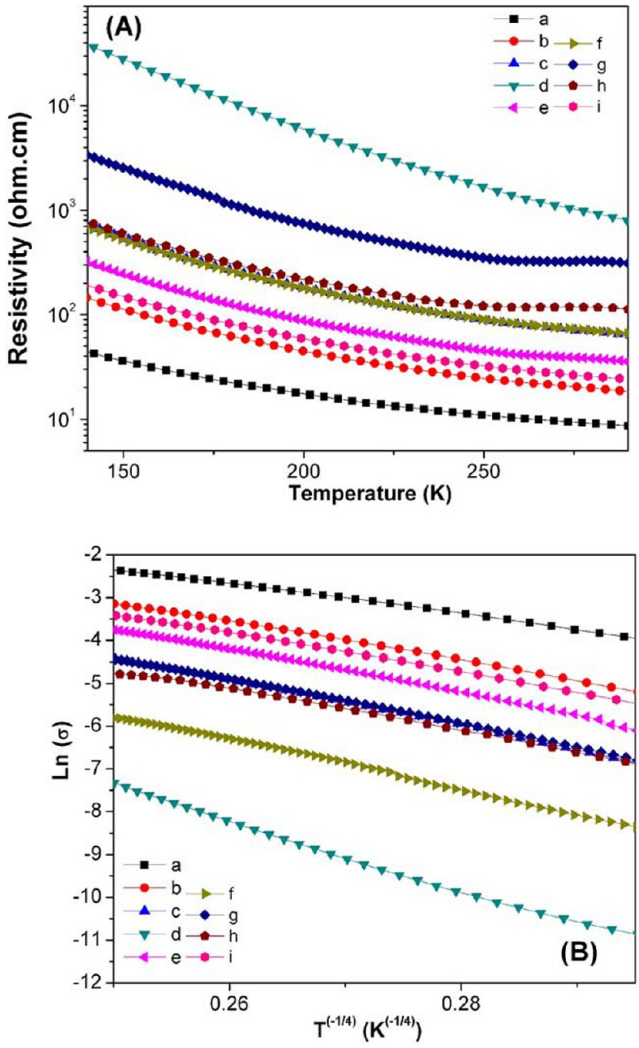

Figure 7. (A) Resistivity vs temperature and (B) $\ln(\sigma)$ vs $T^{-1/4}$ curve of (a) pure PANI; $BaTiO_3$(500 nm)/PANI PNCs with a $BaTiO_3$ loading of (b) 1.0, (c) 5.0, (d) 10.0, (e) 20.0 wt %; (f) $BaTiO_3$(500 nm)/PANI PNCs with a $BaTiO_3$ loading of 20 wt % prepared by physical mixture; (g) $BaTiO_3$(500 nm)/PANI PNCs with a $BaTiO_3$ loading of 20 wt % prepared with combined stirring method; and $BaTiO_3$(100 nm)/PANI PNCs with a $BaTiO_3$ loading of (h) 1.0 and (i) 20 wt %.

Table 2. T_0 and σ_0 for Pure PANI and $BaTiO_3$/PANI NPCs

samples	$T_0 \times 10^5$ (K)	σ_0 (S/cm)
pure PANI	26.40	2480.19
$BaTiO_3$(500 nm)/PANI		
with $BaTiO_3$ loading of 1.0 wt %	43.62	3956.84
with $BaTiO_3$ loading of 5.0 wt %	83.61	8249.43
with $BaTiO_3$ loading of 10.0 wt %	321.93	89769.45
with $BaTiO_3$ loading of 20 wt %	60.36	5518.16
with $BaTiO_3$ loading of 20.0 wt % physical mixture	67.91	4171.37
with $BaTiO_3$ loading of 20.0 wt % prepared by combined stirring methods	98.57	3775.92
$BaTiO_3$(100 nm)/PANI		
with $BaTiO_3$ loading of 1.0 wt %	80.26	5703.30
with $BaTiO_3$ loading of 20.0 wt %	78.73	6998.14

dx.doi.org/10.1021/jp303226u | J. Phys. Chem. C 2012, 116, 15731–15740

10.0 wt %, T_0 increases, and a higher T_0 indicates a stronger localization of the charge carriers, and thus represents a lower σ.[8] In addition, from the aspect of the space charge limited conductivity theory,[52] the resistivity of the $BaTiO_3$/PANI PNCs is largely affected by the thickness of the PANI layer on the $BaTiO_3$ particles.[52] With increasing the loading percentage of the $BaTiO_3$ nanoparticles, the thickness of the PANI layer is decreased as shown in the discussion of the morphology part and thus the resistivity decreases. However, when the loading further increases to 20.0 wt %, both the resistivity and T_0 decrease, which indicates a weaker localization. Due to the ferroelectric property of $BaTiO_3$ NPs[53] and the particle network dependent electron transport behaviors,[54] the resultant electric polarization with an external electric field is helpful for the electron transport on the PANI chains and thus leads to a lower resistivity, Figure 7Ae.

Comparing the sample of $BaTiO_3$(500 nm)/PANI PNCs with a $BaTiO_3$ loading of 20.0 wt %, Figure 7Af,Bf, prepared with physical mix and prepared with chemical coating process, Figure 7Ae,Be, the former sample has higher resistivity and T_0 than the latter one. A higher T_0 indicates an enhanced localization of the charge carriers which is due to the ferroelectric nature of $BaTiO_3$. The resistivity difference of the two samples also demonstrates that the $BaTiO_3$ NPs are well coated by PANI in the chemical method prepared samples.

The $BaTiO_3$(500 nm)/PANI PNCs with a $BaTiO_3$ loading of 20 wt % sample prepared with combined stirring method, Figure 7Ag,Bg, has higher resistivity than the sample prepared only with ultrasonication, Figure 7Ae,Be, which is due to the actual loading of the former sample (32.00 wt %, Table 1) being higher than that of the latter one (28.05 wt %, Table 1), which caused higher space charge.

3.6. Dielectric Permittivity. Figure 8A,B shows the real permittivity (ε') and imaginary permittivity (ε'') of pure PANI and the $BaTiO_3$/PANI PNCs, respectively. Three stages are observed in both ε' and ε'' curves of the PNCs prepared with chemical coating process. The real permittivity ε' first increases rapidly in the lower frequency region (20−110 Hz), and then the increment becomes flat between 110 and 10^5 Hz, finally, in the high frequency region (10^5 to 2×10^6 Hz), ε' has a slight change with increasing frequency, and almost keeps constant. The variation of ε'' with the increase of frequency is contrary to the ε', and at high frequency, the value of ε'' becomes very small and almost equals zero. The same phenomenon also exists in the dielectric loss (tan δ) curve, Figure 8C; in the higher frequency region (10^5 to 2×10^6 Hz) tan δ tends to be zero. Such lower dielectric loss (tan δ) at high frequency can be useful in the supercapacitor field.[8]

The negative real permittivity ε' observed in the PANI particles is due to the delocalization of charges in a macroscopic scale,[55] and related to the instinct metallic state in PANI.[56] However, the delocalization behavior in the mesoscopic range is associated with the ratio of disordered regions in a crystalline structure; the delocalization increases with increasing crystallinity.[56] Thus, the relative lower ε' of $BaTiO_3$(500 nm)/PANI with a $BaTiO_3$ loading of 1 wt % and $BaTiO_3$(100 nm)/PANI with a $BaTiO_3$ loading of 1 wt % sample result from the increment of crystallinity.

The dielectric property of the sample with a loading of 20 wt % prepared by simple physical mixture, Figure 8Af−Cf, has a huge difference from the sample with the same loading prepared by chemical process, Figure 8Ae−Ce. For the physical mix sample, almost in the whole frequency region (110 to 2×10^6 Hz), ε' is positive, and increases sharply in the higher frequency region (10^5 to 2×10^6 Hz). However, the imaginary permittivity ε'', the same as tan δ, tends to be constant with increasing frequency. The positive real permittivity of the physical mixture sample, Figure 8Af−Cf, is attributed to the storage of charge, which is the ferroelectric nature of $BaTiO_3$.[52]

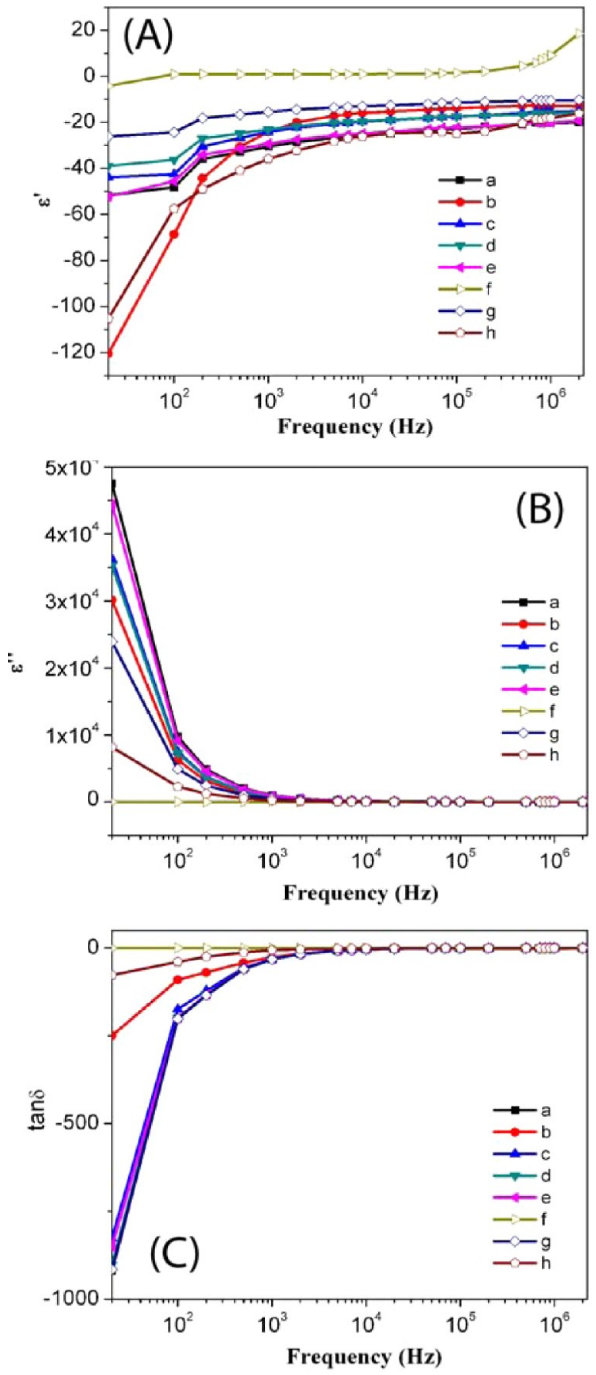

Figure 8. (A) Real permittivity, (B) imaginary permittivity and (C) dielectric loss of (a) pure PANI; $BaTiO_3$(500 nm)/PANI PNCs with a $BaTiO_3$ loading of (b) 1 wt %, (c) 5 wt %, (d) 10.0 wt %, (e) 20.0 wt %; (f) $BaTiO_3$(500 nm)/PANI PNCs with a $BaTiO_3$ loading of 20.0 wt % prepared by physical mixture; (g) $BaTiO_3$(500 nm)/PANI PNCs with a $BaTiO_3$ loading of 20.0 wt % prepared by a combined stirring method; (h) $BaTiO_3$(100 nm)/PANI PNCs with a $BaTiO_3$ loading of 1.0 wt %.

dx.doi.org/10.1021/jp303226u | J. Phys. Chem. C 2012, 116, 15731−15740

Thus, the negative real permittivity of the PNCs indicates that the $BaTiO_3$ particles are well coated with PANI on its surface.

3.7. Magnetoresistance Properties. The magnetoresistance (MR), $R(H,T) - R(0,T)/R(H,T))$, where R is resistance and H is the magnetic field, is defined as a resistance change when the relative orientation of the magnetic domains in adjacent layers is adjusted from antiparallel to parallel under an applied magnetic field.[34] Generally, two models are utilized to explain the resistance variation under an external magnetic field. The negative MR is associated with the forward interference model,[57,58] in which the effect of interference among various hopping paths between hopping sites is considered. Based on eq 3,

$$\frac{\Delta R(H,\,T)}{R(0,\,T)} = \frac{R(H,\,T) - R(0,\,T)}{R(0,\,T)} \approx -C_{sat}\frac{H}{H_{sat}} \qquad (3)$$

C_{sat} is the saturation constant, and H_{sat} is the effective saturation magnetic field; the resistance will decrease with the addition of a magnetic field.

On the contrary, the other theory, i.e., wave function shrinkage model,[58] aims to interpret the positive MR. In this theory, MR is given by eq 4:

$$\frac{\Delta R(H,\,T)}{R(0,\,T)} \approx t_2\frac{H^2}{H_C{}^2}\left(\frac{T_{Mott}}{T}\right)^{1/4} \qquad (4)$$

$t_2 = (5/2016) \times 36$ is a numerical constant, $H_C = 6\hbar[ea_0{}^2(T_{Mott}/T)^{1/4}]$, H_C is the normalized intrinsic magnetic field and a_0 is the localization length. The external magnetic field will contract the electronic wave function at impurity centers, which in turn reduce the hopping probability and further cause the increase of the resistance. The introduction of a magnetic field contracts the localization site and causes the decrease of a_0, which then increases the resistance $R(H,T)$.

For all samples, Figure 9, the MR increases sharply with increasing the magnetic field at the lower magnetic field and the slopes become gentle with further increases of the magnetic field. Under the same magnetic field, the sample with physical mixture of PANI and $BaTiO_3$, Figure 9e, has the highest MR, and pure PANI has higher MR than all the chemically synthesized PNCs. As discussed previously owing to the ferroelectric nature of $BaTiO_3$, the function of the localization of charge carriers will be enhanced and thus causes larger increased resistance. However, when coated with PANI, the PNCs have lower MR, which is even lower than that of pure PANI. This phenomenon indicates that the introduction of $BaTiO_3$ reduces the function of magnetic field on the contraction of the electronic wave function at impurity center, thus the MR of the PNCs is lower than that of pure PANI; and the PANI layer can reduce the ferroelectric property of $BaTiO_3$.

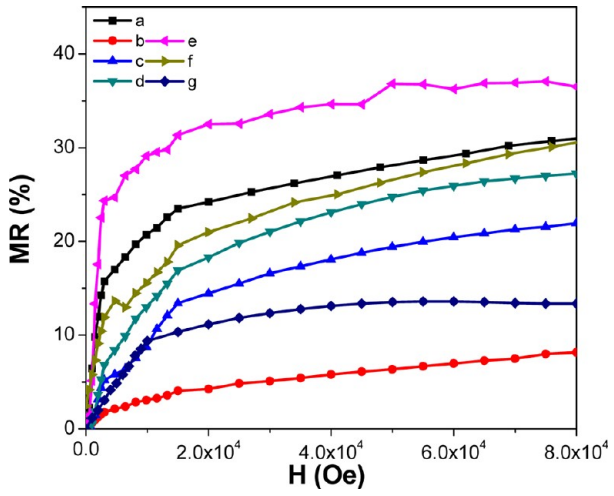

Figure 9. Magnetoresistance of (a) pure PANI; $BaTiO_3$(500 nm)/PANI PNCs with a $BaTiO_3$ loading of (b) 1.0 wt %, and (c) 20.0 wt %; (d) $BaTiO_3$(500 nm)/PANI PNCs with a $BaTiO_3$ loading of 20.0 wt % prepared by physical mixture; (e) $BaTiO_3$(500 nm)/PANI with a $BaTiO_3$ loading of 20.0 wt % prepared with combined stirring method; $BaTiO_3$(100 nm)/PANI PNCs with a $BaTiO_3$ loading of (f) 1.0 wt % and (g) 20.0 wt %.

4. CONCLUSION

A series of $BaTiO_3$/PANI PNCs, synthesized by the surface initial polymerization method, were obtained by varying the $BaTiO_3$ nanoparticle loading, particle size and stirring method. FT-IR analysis indicated a strong interaction between PANI and $BaTiO_3$ nanoparticles in the chemically synthesized nanocomposites. However, no obvious interaction is observed in the sample prepared by the simple physically mixed PANI–$BaTiO_3$ nanocomposites. The effects of the parameters on the crystalline structure, thermal stability, morphology, electrical conductivity and dielectric permittivity are systematically studied. TEM observation reveals a thin PANI coating surrounding the $BaTiO_3$ NPs. The crystallinity of the PNCs is observed to depend on the $BaTiO_3$ loading. In the PNCs with lower loading, for example, 1 wt %, the nanoparticles act as "nucleating sites" for the PANI chains to grow; however, in the PNCs with higher loading (above 5 wt %), the agglomerated nanoparticles block the formation of crystalline structure of PANI. Temperature dependent conductivity test reveals a 3-d VRH electron transport mechanism. The resistivity sharply increases with increasing the $BaTiO_3$ nanoparticle loading from 0.0 to 10 wt %, and the increased resistivity is mainly attributed to the dominating space charges on the interface between $BaTiO_3$ and PANI. However, in higher loading, for example, 20 wt %, the resistivity becomes lower arising from the electric polarization with an external electric field. Compared with the positive dielectric permittivity in the physical mixture sample, all the chemically synthesized PNC samples exhibit a negative dielectric permittivity. Positive magnetoresistance (MR) is also observed in all kinds of PNCs and is analyzed theoretically from the wave function shrinkage model.

AUTHOR INFORMATION

Corresponding Author

*Z.G.: e-mail, zhanhu.guo@lamar.edu; phone, (409) 880-7654. S.W.: e-mail, suying.wei@lamar.edu; phone, (409) 880-7976.

Notes

The authors declare no competing financial interest.

ACKNOWLEDGMENTS

This project is supported by the National Science Foundation-Nanoscale Interdisciplinary Research Team and Materials Processing and Manufacturing (CMMI 10-30755) managed by Dr. Mary Toney. D.P.Y. acknowledges support from the NSF under Grant No. DMR 04-49022. S.W. acknowledges the Welch foundation (V-0004).

REFERENCES

(1) Zhu, J.; Wei, S.; Chen, X.; Karki, A. B.; Rutman, D.; Young, D. P.; Guo, Z. *J. Phys. Chem. C.* **2010**, *114*, 8844−8850.
(2) Zhong, L.-S.; Hu, J.-S.; Cao, A.-M.; Liu, Q.; Song, W.-G.; Wan, L.-J. *Chem. Mater.* **2007**, *19*, 1648−1655.
(3) Shen, J.; Shi, M.; Li, N.; Yan, B.; Ma, H.; Hu, Y.; Ye, M. *Nano Res.* **2010**, *3*, 339−349.
(4) Li, Y.; Shimizu, H. *Macromolecules* **2009**, *42*, 2587−2593.
(5) Li, X.; Chang, W.-C.; Chao, Y. J.; Wang, R.; Chang, M. *Nano Lett.* **2004**, *4*, 613−617.
(6) Yu, Y.; Che, B.; Si, Z.; Li, L.; Chen, W.; Xue, G. *Synth. Met.* **2005**, *150*, 271−277.
(7) Deng, J.; Ding, X.; Zhang, W.; Peng, Y.; Wang, J.; Long, X.; Li, P.; Chan, A. S. C. *Polymer* **2002**, *43*, 2179−2184.
(8) Zhu, J.; Wei, S.; Zhang, L.; Mao, Y.; Ryu, J.; Karki, A. B.; Young, D. P.; Guo, Z. *J. Mater. Chem.* **2011**, *21*, 342−348.
(9) Yong, V.; Hahn, H. T. *J. Mater. Res.* **2009**, *24*, 1553−1558.
(10) Gu, H.; Huang, Y.; Zhang, X.; Wang, Q.; Zhu, J.; Shao, L.; Haldolaarachchige, N.; Young, D. P.; Wei, S.; Guo, Z. *Polymer* **2012**, *53*, 801−809.
(11) Ding, K.; Jia, H.; Wei, S.; Guo, Z. *Ind. Eng. Chem. Res.* **2011**, *50*, 7077−7082.
(12) Xian, Y.; Hu, Y.; Liu, F.; Xian, Y.; Wang, H.; Jin, L. *Biosens. Bioelectron.* **2006**, *21*, 1996−2000.
(13) Wu, S.; Ju, H. X.; Liu, Y. *Adv. Funct. Mater.* **2007**, *17*, 585−592.
(14) Fu, H.; Bellaiche, L. *Phys. Rev. Lett.* **2003**, *91*, 257601.
(15) Roberts, S. *Phys. Rev.* **1947**, *71*, 890.
(16) Windlass, H.; Raj, P. M.; Balaraman, D.; Bhattacharya, S. K.; Tummala, R. R. *IEEE Trans. Electron. Packag. Manuf.* **2003**, *26*, 100−105.
(17) Kobayashi, Y.; Tanase, T.; Tabata, T.; Miwa, T.; Konno, M. *J. Eur. Ceram. Soc.* **2008**, *28*, 117−122.
(18) Kobayashi, Y.; Kosuge, A.; Konno, M. *Appl. Surf. Sci.* **2008**, *255*, 2723−2729.
(19) Wang, J.; Lin, Q.; Zhou, R.; Xu, B. *Appl. Surf. Sci.* **2002**, *81*, 248−253.
(20) Jung, H. M.; Kang, J.-H.; Yang, S. Y.; Won, J. C.; Kim, Y. S. *Chem. Mater.* **2009**, *22*, 450−456.
(21) Moon, H.-S.; Park, J.-K. *Synth. Met.* **1998**, *92*, 223−228.
(22) Tarver, J.; Yoo, J. E.; Dennes, T. J.; Schwartz, J.; Loo, Y.-L. *Chem. Mater.* **2008**, *21*, 280−286.
(23) Yoo, J. E.; Cross, J. L.; Bucholz, T. L.; Lee, K. S.; Espe, M. P.; Loo, Y.-L. *J. Mater. Chem.* **2007**, *17*, 1268−1275.
(24) Yang, X.; Li, B.; Wang, H.; Hou, B. *Prog. Org. Coat.* **2007**, *69*, 267−271.
(25) Dhawan, S. K.; Kumar, D.; Ram, M. K.; Chandra, S.; Trivedi, D. C. *Sens. Actuators, B* **1997**, *40*, 99−103.
(26) Olad, A.; Nabavi, R. *J. Hazard. Mater.* **2007**, *147*, 845−851.
(27) Li, M.; Guo, Y.; Wei, Y.; MacDiarmid, A. G.; Lelkes, P. I. *Biomaterials* **2006**, *27*, 2705−2715.
(28) Virji, S.; Huang, J.; Kaner, R. B.; Weiller, B. H. *Nano Lett.* **2004**, *4*, 491−496.
(29) Zhang, X.; Zhu, J.; Haldolaarachchige, N.; Ryu, J.; Young, D. P.; Wei, S.; Guo, Z. *Polymer* **2012**, *53*, 2109−2120.
(30) Chuang, F.-Y.; Yang, S.-M. *J. Colloid Interface Sci.* **2008**, *320*, 194−201.
(31) Abbas, S. M.; Dixit, A. K.; Chatterjee, R.; Goel, T. C. *Mater. Sci. Eng. B* **2005**, *123*, 167−171.
(32) Wei, J. H.; Shi, J.; Guan, J. G.; Yuan, R. Z. *J. Mater. Sci.* **2004**, *39*, 3457−3460.
(33) Pant, H. C.; Patra, M. K.; Verma, A.; Vadera, S. R. *Acta Mater.* **2006**, *54*, 3163−3169.
(34) Baibich, M. N.; Broto, J. M.; Fert, A.; Van Dau, F. N.; Petroff, F.; Etienne, P.; Creuzet, G.; Friederich, A.; Chazelas, J. *Phys. Rev. Lett.* **1988**, *61*, 2472.
(35) Prigodin, V. N.; Bergeson, J. D.; Lincoln, D. M.; Epstein, A. J. *Synth. Met.* **2006**, *156*, 757−761.
(36) Bloom, F. L.; Wagemans, W.; Kemerink, M.; Koopmans, B. *Phys. Rev. Lett.* **2007**, *99*, 257201.
(37) Wagemans, W.; Schellekens, A. J.; Kemper, M.; Bloom, F. L.; Bobbert, P. A. *Phys. Rev. Lett.* **2011**, *106*, 196802.
(38) Xiong, Z. H.; Wu, D.; Valy Vardeny, Z.; Shi, J. *Nature* **2004**, *427*, 821−824.
(39) Zhu, J.; Zhang, X.; Haldolaarachchige, N.; Wang, Q.; Luo, Z.; Ryu, J.; Young, D. P.; Wei, S.; Guo, Z. *J. Mater. Chem.* **2012**, *22*, 4996−5005.
(40) Zhu, J.; Wei, S.; Haldolaarachchige, N.; He, J.; Young, D. P.; Guo, Z. *Nanoscale* **2012**, *4*, 152−156.
(41) Zhu, J.; Wei, S.; Ryu, J.; Guo, Z. *J. Phys. Chem. C* **2011**, *115*, 13215−13222.
(42) Hoffman, A. J.; Alekseyev, L.; Howard, S. S.; Franz, K. J.; Wasserman, D.; Podolskiy, V. A.; Narimanov, E. E.; Sivco, D. L.; Gmachl, C. *Nat. Mater.* **2007**, *6*, 946−950.
(43) Pendry, J. B.; Holden, A. J.; Stewart, W. J.; Youngs, I. *Phys. Rev. Lett.* **1996**, *76*, 4773.
(44) Dolgov, O. V.; Kirzhnits, D. A.; Maksimov, E. G. *Rev. Mod. Phys.* **1981**, *53*, 81.
(45) Zhu, J.; Wei, S.; Zhang, L.; Mao, Y.; Ryu, J.; Haldolaarachchige, N.; Young, D. P.; Guo, Z. *J. Mater. Chem.* **2011**, *21*, 3952−3959.
(46) Lee, K.; Cho, S.; Heum Park, S.; Heeger, A. J.; Lee, C.-W.; Lee, S.-H. *Nature* **2006**, *441*, 65−68.
(47) Éfendiev, É. G.; Gadzhieva, N. N.; Il'yasly, T. M.; Abbasova, R. F.; Yakh'yaev, F. F. *J. Appl. Spectrosc.* **2006**, *73*, 462−465.
(48) Pouget, J. P.; Jozefowicz, M. E.; Epstein, A. J.; Tang, X.; MacDiarmid, A. G. *Macromolecules* **1991**, *24*, 779−789.
(49) Lu, X.; Ng, H. Y.; Xu, J.; He, C. *Synth. Met.* **2002**, *128*, 167−178.
(50) Chen, T.; Dong, C.; Li, X.; Gao, J. *Polym. Degrad. Stab.* **2009**, *94*, 1788−1794.
(51) Guo, Z.; Shin, K.; Karki, A.; Young, D.; Kaner, R.; Hahn, H. *J. Nanopart. Res.* **2009**, *11*, 1441−1452.
(52) Patil, R. C.; Radhakrishnan, S.; Pethkar, S.; Vijaymohanan, K. *J. Mater. Res.* **2001**, *16*, 1982−1988.
(53) Yun, W. S.; Urban, J. J.; Gu, Q.; Park, H. *Nano Lett.* **2002**, *2*, 447−450.
(54) Zhu, J.; Wei, S.; Zhang, L.; Mao, Y.; Ryu, J.; Mavinakuli, P.; Karki, A. B.; Young, D. P.; Guo, Z. *J. Phys. Chem. C* **2001**, *114*, 16335−16342.
(55) Liu, C.-D.; Lee, S.-N.; Ho, C.-H.; Han, J.-L.; Hsieh, K.-H. *J. Phys. Chem. C* **2008**, *112*, 15956−15960.
(56) Joo, J.; Oh, E. J.; Min, G.; MacDiarmid, A. G.; Epstein, A. J. *Synth. Met.* **1995**, *69*, 251−254.
(57) Jaiswal, M.; Wang, W.; Fernando, K. A. S.; Sun, Y.-P.; Menon, R. *Phys. Rev. B* **2007**, *76*, 113401.
(58) Su, T.-I.; Wang, C.-R.; Lin, S.-T.; Rosenbaum, R. *Phys. Rev. B* **2002**, *66*, 054438.